Degradation non-uniformity in the solar diffuser bidirectional reflectance distribution function

Junqiang Sun[1,2], Mike Chu[1,3] and Menghua Wang[1]

[1]NOAA National Environmental Satellite, Data, and Information Service
Center for Satellite Applications and Research
E/RA3, 5830 University Research Ct., College Park, MD 20740, USA

[2]Global Science and Technology, 7855 Walker Drive, Suite 200, Maryland, USA
[3]Cooperative Institute for Research in the Atmosphere, Colorado State University, Fort Collins, Colorado

ABSTRACT

The assumption of angular dependence stability of the solar diffuser (SD) through out degradation is critical to the on-orbit calibration of the reflective solar bands (RSB) in many satellite sensors. Recent evidence has pointed to the contrary, and in this work we present a thorough investigative effort into the angular dependence of the SD degradation for the Visible Infrared Imaging Radiometer Suite (VIIRS) onboard Suomi National Polar-orbiting Partnership (SNPP) satellite and for the twin Moderate-resolution Imaging Spectroradiometer (MODIS) onboard Terra and Aqua spacecrafts. One common key step in the RSB calibration is the use of the SD degradation performance measured by an accompanying solar diffuser stability monitor (SDSM) as a valid substitute for the SD degradation factor in the direction of the RSB view. If SD degradations between these two respective directions do not maintain the same relative relationship over time then the unmitigated use of the SDSM-measured SD degradation factor in the RSB calibration calculation will generate bias and consequently long-term drift in derived science products. We exploit the available history of the on-orbit calibration events to examine the response of the SDSM and the RSB detectors to the incident illumination reflecting off SD versus solar declination angle and show that the angular dependency, particularly at short wavelengths, evolves with respect to time. The generalized and the decisive conclusion is that

the bidirectional reflectance distribution function (BRDF) of the SD degrades non-uniformly with respect to both incident and outgoing directions. Thus, the SDSM-based measurements provide SD degradation factors that are biased relative to the RSB view direction with respect to the SD. The analysis also reveals additional interesting phenomena, for example, the sharp behavioral change in the evolving angular dependence observed in Terra MODIS and SNPP VIIRS. For SNPP VIIRS the mitigation for this "*SD degradation non-uniformity effect*" with respect to angles relies on a "Hybrid Methodology" using lunar-based calibration to set the reliable long-term baseline. For MODIS, the use of earth targets in the major release Collection 6 to improve calibration coefficients and time-dependent response-versus-scan-angle (RVS) characterization inherently averts the use of SD and its associated issues. The work further supports that having an open-close operational capability for the space view door can minimize SD degradation and its associated effects due to solar exposure, and thus provide long-term benefits for maintaining calibration and science data accuracy.

Keywords: VIIRS, MODIS, Solar diffuser, Solar diffuser stability monitor, SD degradation, Reflective solar bands, Bidirectional reflectance distribution function, Non-uniformity

1. Introduction

The solar diffuser (SD) has been an integral part of the onboard calibration of the solar reflective bands (RSB) of many major satellite sensors that are at the heart of the global environmental observation and major Earth science output [1-8]. The SD is a space-grade reflector made of Spectralon with very high diffuse reflectance that is near-Lambertian [9]. Figure 1 is the image of the Visible Infrared Imaging Radiometer Suite (VIIRS) SD [5]. The simple and near-ideal reflectance property of an SD makes it a useful onboard calibrator of a satellite sensor and provides a straightforward calibration methodology to make regular updates of the on-orbit RSB calibration. However, recent investigations by Sun and Wang [6, 10, 11] have uncovered evidence of evolving angular dependence in the degradation of SD reflectance

that invalidates a key assumption in the SD-based calibration methodology. In this extended investigative effort into this key property of the SD reflectance we examine the calibration data from VIIRS onboard Suomi National Polar-orbiting Partnership (SNPP) satellite and from the twin Moderate-resolution Imaging Spectroradiometer (MODIS) onboard Terra and Aqua spacecrafts. Common to the RSB calibration of these three instruments is their core calibration procedure and input components that are essentially identical [1, 2, 4-8], including the key assumption that the on-orbit degradation of SD reflectance will retain the same angular dependence with respect to incoming and outgoing angles. Our examination into the calibration data from these three different instruments, which follow identical procedure to generate RSB calibration coefficients, then can reveal the property of SD common to all three.

Figure 2 is a schematic of the SNPP VIIRS layout that shows the relevant components for this analysis. For MODIS, the layout has some differences but in the context of this work the involved components and the procedure are identical. The RSB calibration methodology is based on the premise that SD provides incident illumination to the RSB that is accurately quantified, and against this reference the RSB then can be calibrated [1, 2, 4-8]. Due mainly to ultraviolet light exposure, contaminants and high-energy particles [12], the on-orbit reflectance performance of the SD degrades, thus an accurate determination of the degradation of the SD at regular timed intervals is central to RSB calibration. An accompanying spectral radiometer called the solar diffuser stability monitor (SDSM) [10, 13-15] achieves this purpose via regularly scheduled measurement operations. In reality, the SDSM tracks the SD degradation only in the outgoing SDSM view direction and there is otherwise no capability to make direct measurement of the on-orbit SD degradation in the RSB direction. Despite this difference in angles that can lead to bias, the standard methodology simply applies the SD degradation analysis result from the SDSM to the RSB calibration calculation [1, 2, 4-8], thus implicitly assuming that the SD degradation toward RSB and the SD degradation toward SDSM are interchangeable, and is to

remain so all throughout degradation history. As the incident and the outgoing angles used in this analysis are not deemed uniquely special, a more meaningful generalization of this idealized condition is that the angle-dependence of the bidirectional reflectance distribution function (BRDF) of the SD will remain unchanged. Under this generalization, what is expected to change is the overall reflectance of the BRDF due to performance degradation, and this can be characterized by a single time-dependent degradation factor and be measured by the SDSM [10, 13-15]. The characteristic of the degradation of SD since launch, and not the BRDF itself, is the focus of this examination. As mentioned previously, the Sun and Wang analysis has already uncovered evidence of changing angular dependence in SD degradation in SNPP VIIRS. In the context of this paper, we use the term "*degradation non-uniformity*" to describe the non-trivial change in the relative angular dependence in the SD degradation with respect to time that contributes to the absolute anisotropy of its BRDF.

For SNPP VIIRS, its SD reflectance performance has already degraded ~30% in just over four years [10], and SD-based RSB calibration results in the past several years have already suggested bias, or inaccuracy, of up to ~1% against lunar-based analysis [11]. Recent deep dive investigations have successfully identified the effect of SD degradation non-uniformity affecting both VIIRS RSB calibration and the ocean color products that are highly sensitive to sensor data accuracy especially for the short wavelength visible bands [16-21]. The same analyses also led to a mitigation approach that mixes in lunar observations to establish the correct long-term SD degradation baseline in a so-called "Hybrid Method" to restore RSB calibration accuracy [11, 22]. This work aims to expand the scope for a thorough exposition of the effect. For Terra and Aqua MODIS, no previous examination of the effect has been performed, but their on-orbit calibration results have indeed shown bias since early mission and that the bias has progressively worsened. The bias is especially strong for Terra MODIS short wavelength bands, for example by as much as ~10% for the shortest wavelength, or the 412 nm band [24] in the SD-based

calibration. While the reason for the bias was unknown at the time, MODIS Collection 6 (C6) by *Sun et al.* [24, 25], released in 2011, abandoned the use of SD methodology for short-wavelength bands and instead turned to earth targets to provide an improved characterization of the calibration coefficients and also the time-dependent response-versus-angle (RVS) effect. The fix for the affected bands is provided by the MODIS C6 methodology by simply adapting to an entirely different calibration source. This work extends the scope of Sun and Wang's analysis [6, 9, 10] mentioned previously for a dedicated study of the SD degradation non-uniformity effect in SNPP VIIRS, Terra MODIS and Aqua MODIS. With Terra MODIS operating for more than 15 years and Aqua MODIS for more than 13 years [1, 2], their long mission history provides very extensive information under a greater variety of different conditions. The result from this dedicated analysis will explicitly reveal that the SD degradation non-uniformity effect exists in MODIS SD and is one of primary contributors to the failure of the MODIS RSB calibration, especially at short wavelengths. For the three sensors here considered, the effect generates an underlying calibration inaccuracy that will propagate through the pipeline into the products leading to long-term drift and erroneous scientific results.

The paper is organized as follows. Section 2 briefly describes the calibration methodology relevant for this analysis, for both SDSM and RSB measurements. Section 3 shows SDSM and RSB data and results for SNPP VIIRS. Section 4 presents RSB data and result for Terra and Aqua MODIS. Section 5 discusses general issues for the SD degradation non-uniformity effect, various challenges and related key issues, and mitigation method for both MODIS and VIIRS. Section 6 concludes this work.

2. Algorithm and Procedure

A description is provided for the essential components in the RSB calibration with emphasis on those relevant to this specialized analysis. We highlight the property of the on-orbit change

of the SD reflectance and how the degradation non-uniformity effect is characterized. The algorithm and analysis procedure are separately presented for SDSM and RSB.

A. General Instrument Layout and Calibration Description

The reflectance property of a surface is characterized by a BRDF that is a function of both incident and outgoing angles. The BRDF value at a given outgoing direction is called the bidirectional reflectance factor (BRF), which is its BRDF multiplied by a factor of π, i.e., πxBRF. The BRF of the SD in the RSB view direction for both MODIS and VIIRS is measured prelaunch and also validated on-orbit using the measurements from planned yaw maneuvers [26-30]. For the BRF of the SD in the SDSM direction only the relative BRF, which differs from the absolute BRF by a constant factor, is needed and can be derived from planned on-orbit yaw measurements, which have been performed for both MODIS instruments and SNPP VIIRS [29-30]. It can also be measured pre-launch as in SNPP VIIRS. In practice, for the SDSM only the relative BRF with respect to an initial time is needed for the SDSM calibration analysis to track the on-orbit performance change of the SD [10, 13-15].

Figure 3 displays a schematic of on-orbit calibration involving the SD, SDSM, RSB, and the two view ports – the SDSM sun-view (SV) port and the SD port - where sunlight passes through. For SNPP VIIRS, the RSB views the SD through the rotating telescope assembly (RTA) [31]. There is an SDSM SV screen (SVS) for the SV port and an SD screen (SDS) for the SD port that can be operated in a closed or screened position to prevent saturation of detectors from excessive solar exposure [1, 2]. The SDS impacts the solar illumination reaching the SD and this effect will also be addressed in this work. SNPP VIIRS is actually designed with a permanently fixed SDS without an SD door [31], but MODIS SDS was designed with an SD door that can operate in one of three modes: door closed, door open with SDS screened, and door open with SDS open. However, Terra MODIS has operated only in permanent screened mode following the 2007 SD door anomaly [1, 2]. The SDSM measures the light coming from the SD to compare with the direct sunlight coming from the SVS port to track the relative change of the SD reflectance over

time, characterized as SD degradation. The SDSM measurement of the SD reflectance performance is typically carried out frequently during early mission and then the frequency is gradually reduced to a stable level depending on needs and operation schedule [10, 13]. The use of the SD degradation measured by the SDSM as an input for the RSB view in the RSB coefficient calculation is at the heart of this examination.

B. General SD Degradation

The BRDF of SD at a wavelength λ can be separated into a product of an initial component and a time-dependent component,

$$BRDF(\theta_{in},\phi_{in},\theta_{out},\phi_{out},\lambda,t) = BRDF(\theta_{in},\phi_{in},\theta_{out},\phi_{out},\lambda,t_0) \cdot \Delta BRDF(\theta_{in},\phi_{in},\theta_{out},\phi_{out},\lambda,t), \quad (1)$$

where θ_{in} and ϕ_{in} are two independent angles to describe the incident direction of light on the SD surface, θ_{out} and ϕ_{out} are the angles for the outgoing direction, t_0 is any selected initial time, and $\Delta BRDF(\theta_{in},\phi_{in},\theta_{out},\phi_{out},\lambda,t)$ is the SD BRDF degradation factor at time t since time t_0. The two angles can be solar declination, solar azimuth or any two independent solar angles in the instrument coordinate system. As demonstrated in Fig. 3, two outgoing directions are involved in an SD calibration and SDSM calibration event - one towards the SDSM and the other towards the RSB (or RTA in case of VIIRS). As previously mentioned, when the outgoing direction is fixed, e.g. with θ_{out} and ϕ_{out} pointing toward a specific component, the BRF is the relevant quantity. The expression for the BRF can be reworked from Eq. (1) as

$$BRF_{SDSM}(\theta_{in},\phi_{in},\lambda,t) = BRF_{SDSM}(\theta_{in},\phi_{in},\lambda,t_0) \cdot \Delta BRF_{SDSM}(\theta_{in},\phi_{in},\lambda,t) \quad (2)$$

for the SDSM view direction and

$$BRF_{RSB}(\theta_{in},\phi_{in},\lambda,t) = BRF_{RSB}(\theta_{in},\phi_{in},\lambda,t_0) \cdot \Delta BRF_{RSB}(\theta_{in},\phi_{in},\lambda,t) \quad (3)$$

for the RSB view direction, where $\Delta BRF_{SDSM}(\theta_{in},\phi_{in},\lambda,t_0)$ and $\Delta BRF_{RSB}(\theta_{in},\phi_{in},\lambda,t_0)$ are the SD degradation for the SDSM and the RSB view directions, respectively. Due to the lack of the

capability to characterize the SD degradation between the prelaunch measurements and the launch time, the launch time is the earliest time for which the SD degradation can be characterized. In fact, the SD is well protected during this period and thus it is standard practice to assume that the SD degradation during this time is small. Thus, t_0 is always chosen as the launch time of the instrument in practice. $BRF_{RSB}(\theta_{in},\phi_{in},\lambda,t_0)$, the characterized result at the initial time, is measured prelaunch and later validated post-launch using the on-orbit measurements from specially planned satellite yaw maneuvers. $BRF_{SDSM}(\theta_{in},\phi_{in},\lambda,t_0)$ can also be measured prelaunch and validated on-orbit with yaw measurements such as was done for SNPP VIIRS. For the on-orbit calibration of SDSM, only the relative BRF is required. Since the relative BRF can be derived from the on-orbit yaw measurements, the prelaunch measurement for $BRF_{SDSM}(\theta_{in},\phi_{in},\lambda,t_0)$ is not explicitly needed for the on-orbit calibration of SDSM although it is essential for other calibration purposes including confirmation with the yaw measurement result and the subsequent analysis [10].

If the statement that the SD degrades uniformly with respect to incident and outgoing directions is accepted, then this implies that the degradation $\Delta BRDF(\theta_{in},\phi_{in},\theta_{out},\phi_{out},\lambda,t)$ can be denoted simply as $\Delta BRDF(\lambda,t)$ without angular dependence. Thus $\Delta BRF_{SDSM}(\theta_{in},\phi_{in},\lambda,t)$ and $\Delta BRF_{RSB}(\theta_{in},\phi_{in},\lambda,t)$ can be expressed as $\Delta BRF_{SDSM}(\lambda,t)$ and $\Delta BRF_{RSB}(\lambda,t)$, respectively, and furthermore would be identical as $\Delta BRF(\lambda,t)$ since there is also no difference between the direction of the RSB and SDSM under the uniformity condition. In this ideal case, the SD degradation for the RSB view direction, the required input in the standard calibration methodology, can then be replaced by the result for the SDSM view direction, which is tracked and measured by the on-orbit SDSM calibration operations. Thus, SD degradation uniformity is a key condition in the standard SD/SDSM methodology for the on-orbit calibration of the RSB. In the MODIS community, the SD degradation is denoted by $\Delta(\lambda,t)$, while in the VIIRS community it is denoted by $H(\lambda,t)$, called H-factors. This of course assumes negligible SD

degradation from time of the prelaunch measurement to the launch time, after which $\Delta BRF(\lambda,t)$ characterizes the SD degradation since launch.

In a calibration event as illustrated in Fig. 3, the sunlight passing through the SD port reflects off the SD to reach the SDSM and the RSB. The SDSM, in principle as previously mentioned, measures the time-dependent overall reflectance level $\Delta BRF(\lambda,t)$ of the SD during specially scheduled operations. The calibration coefficient for the RSB is then calculated using $\Delta BRF(\lambda,t)$ as the reference input for the updated SD performance. For either the SDSM or RSB, the calibration measurement event occurs in a short window of time several minutes before the satellite crosses the terminator from the nightside of the Earth to the dayside, as shown in Fig. 4. Due to the changing orientation and the position of the spacecraft, the incident angle of the sunlight impinging on the SD can vary over a small range of angles during the full-illumination stage of the SD. Within this full-illumination range, a narrower interval called a "sweet spot" [6, 10], and its corresponding SDSM or RSB scans are selected for calibration analysis (see Figs. 6 and 10). Both the SD degradation and the RSB calibration coefficients can be calculated from the data of each scan. If the SD degrades uniformly, the derived SD degradation and the calibration coefficients would show no dependence on the scans provided that the prelaunch BRFs and vignetting function (VF) of the screen in the front of the SD port are accurate. If the prelaunch BRFs and the VF have not been accurately characterized, then the residual errors would then lead to fluctuations that follow yearly cycles due to dependence on orbital and other geometrical conditions. The appearance of fluctuations or drifts is on one hand a check on the quality of the key calibration inputs and on the other a basis to look for changing trends beyond the yearly fluctuations. In the current standard procedure, the dependence is not checked and a simple average over the scans is applied to generate the SD degradation factor or the RSB calibration coefficient for the event.

In this analysis, the angular variation within each calibration event is explicitly exploited to reveal the changing angular dependence in the SD degradation over time caused by the degradation non-uniformity effect in both the RSB and the SDSM responses. Embedded within the selected scans of each calibration event is the information on how detector response depends on the incident angle, and whether or not this dependence change from one event to another is consistent with the assumptions made in the calibration algorithm. In the subsections, we present the key procedural steps within the SD-based calibration pipeline involving the BRF that are essential to demonstrate the effect for all three sensors. The data analysis of the SDSM or the RSB response is same for both VIIRS and MODIS.

C. SDSM Algorithms and the Degradation Non-uniformity Characterization

A linear approximation is applied to characterize the relationship between the incident sunlight and the SDSM response [10, 13], i.e.,

$$L_{SD}(Sample, Scan, D) = Q(D) \cdot dc_{SD,D}(Sample, Scan), \tag{4}$$

where *Sample* and *D* are the SDSM sample number and detector number, L_{SD}(*Sample,Scan,D*) is the radiance reflected off the SD observed by the SDSM detector *D* at the sample of the scan, *Q*(*D*) is the calibration coefficient of SDSM detector *D*, which is inversely proportional to the gain of the detector, and $dc_{SD,D}$(*Sample,Scan*) is the background-subtracted SDSM detector D response for the SD view given as digital counts (dc). The SD-scattered sunlight radiance on left-hand side of Eq. (4) is related to various physical parameters as [10, 13]

$$\begin{aligned} L_{SD}(Sample, Scan, D) = {} & BRF_{SDSM}^{Prl}(\theta_{in}, \phi_{in}, \lambda_D) \cdot \Delta BRF_{SDSM}(\theta_{in}, \phi_{in}, \lambda_D, t) \\ & \cdot \tau_{SDS}(\theta_{in}, \phi_{in}) \cdot \cos(\theta_{SD}) \cdot \varepsilon_{Sun}(\lambda_D) / d_{ES}^2, \end{aligned} \tag{5}$$

where λ_D is the center wavelength of the SDSM detector *D*, $BRF_{SDSM}^{Prl}(\theta_{in}, \phi_{in}, \lambda_{SD})$ is the measured pre-launch BRF (the BRF at time t_0) with outgoing direction toward the SDSM for the detector *D*, $\tau_{SDS}(\theta_{in}, \phi_{in})$ is the VF characterizing the vignetting effect of the SD screen (SDS) in

front of the SD port, θ_{SD} is the angle with respect to the SD normal, d_{ES} is the Earth-Sun distance in Astronomical Unit (AU), and $\varepsilon_{Sun}(\lambda_B)$ is the solar radiance reflecting normal from a 100% Lambertian surface at the Earth-Sun distance of one AU. The vignetting effect is geometrical in nature and should not change with time or wavelength. As already mentioned, $\tau_{SDS}(\theta_{in}, \phi_{in})$ can be measured prelaunch and validated on-orbit using the yaw measurements, or directly measured on orbit [29, 30, 32]. In some events, such as in some MODIS calibration operations for which the SDS is placed in the open position for the SD port and thus devoid of the vignetting effect, then in place of τ_{SDS} would instead be a constant of 1.

By combining the above two expressions, we obtain an expression for the degradation in the direction of the SDSM as

$$\Delta BRF_{SDSM}(\theta_{in}, \phi_{in}, \lambda_D, t) = \frac{Q(D) \cdot \left\langle dc_{SD,D}(Sample, Scan) \right\rangle_{Sample} \cdot d_{ES}^2}{BRF_{SDSM}^{Prl}(\theta_{in}, \phi_{in}, \lambda_D) \cdot \tau_{SDS}(\theta_{in}, \phi_{in}) \cdot \cos(\theta_{SD}) \cdot \varepsilon_{Sun}(\lambda_D)}, \qquad (6)$$

where $<\ldots>_{Sample}$ indicates the average over the SDSM samples. The right side of Eq.(6) is the formula used to track the SD degradation before averaging over scans in the sweet spot in the standard SDSM calibration, but with the caveat that $Q(D)$ is not needed in the actual calculation since only relative degradation is needed. As discussed above, $\Delta BRF_{SDSM}(\theta_{in}, \phi_{in}, \lambda_D, t)$ should remain constant over an individual calibration event if both the SD degrades uniformly and the SD BRF and the SDS VF characterization from prelaunch measurements are accurate. If the SD indeed degrades non-uniformly, then the degradation would change with scans or the incident angle and, furthermore, the changing trend will manifest in a long-term pattern different from the yearly oscillation. In any individual calibration event, because the locus of incident light traces out a specific trajectory, the two angles corresponding to the calibration measurements become dependent of each other. In this analysis, we choose the solar declination angle in the instrument coordinate system to represent the incident angle upon the SD to characterize and demonstrate the non-uniformity effect in each individual event. This is because the solar declination varies

along the path of the trajectory of the solar incidence during the short calibration interval. Then we can write, to first order approximation, the characterization as [10]

$$\Delta BRF_{SDSM}(\theta_{in},\phi_{in},\lambda_D,t) = a(\lambda,t)\left[1+b(\lambda,t)(\phi_{in}-\phi_0)\right] \qquad (7)$$

where ϕ_{in} is the solar declination angle in the instrument coordinate system, ϕ_0 is a reference angle which is 13° for VIIRS and 14.2° for MODIS, respectively, and the coefficient $b(\lambda,t)$ is the newly added parameter to quantify the degree of the angular dependence and its evolution.

D. RSB Algorithm and the Degradation Non-uniformity Characterization

For VIIRS, a quadratic approximation is used to characterize the relationship between the incident sunlight and the instrument response for RSBs [6], i.e.,

$$L_{SD}(Sample,Scan,D,B) = F(B,D,M,G)\cdot\sum_{j=0}^{2} c_j(B,D,M,G)\cdot dn_{SD,B}^{j}(Sample,Scan,D), \qquad (8)$$

where B is the band number, D is the detector number of the band B, *Sample* is the sample number, *Scan* is the scan number, $L_{SD}(Sample,Scan,D,B)$ is the radiance at the sample of the scan observed by detector D of band B, M is the mirror side of the half-angle mirror (HAM) at the scan, and G is the gain status of the detector at the sample of the scan. $F(B,D,M,G)$ is the calibration coefficient, called F-factor, of band B, detector D, mirror side M, and gain G, which is inversely proportional to the on-orbit gain change of the detector of the band. $c_0(B,D,M,G)$, $c_1(B,D,M,G)$, $c_2(B,D,M,G)$ are temperature effect-corrected prelaunch measured calibration coefficients with a quadratic relationship between the background-subtracted instrument response and radiance applied. The term $dn_{SD,B}^{j}(Sample,Scan,D)$ is background-subtracted instrument response. In addition, the SD scattered sunlight radiance, on the left-hand side of Eq. (8), has dependence on various physical parameters as [6]

$$L_{SD}(Sample, Scan, D, B) = \frac{\tau_{SDS}(\theta_{in}, \phi_{in}) \cdot \cos(\theta_{SD})}{d_{ES}^2} \cdot \frac{\int \varepsilon_{Sun}(\lambda_D) \cdot RSR_B(\lambda) \cdot BRF_{RSB}^{Prl}(\theta_{in}, \phi_{in}, \lambda) \cdot \Delta BRF_{RSB}(\theta_{in}, \phi_{in}, \lambda, t) d\lambda}{\int RSR_B(\lambda) d\lambda} \quad (9)$$

where $BRF_{RSB}^{Prl}(\theta_{in}, \phi_{in}, \lambda_{SD})$ is the prelaunch measured SD BRF for the RSB view direction. From Eqs. (8) and (9), we get the full expression for the calibration coefficient,

$$F(B, D, M, G) = \frac{\tau_{SDS}(\theta_{in}, \phi_{in}) \cdot \cos(\theta_{SD})}{d_{ES}^2 \cdot \sum_{j=0}^{2} c_j(B, D, M, G) \cdot dn_{SD,B}^j(Sample, Scan, D)} \cdot \frac{\int \varepsilon_{Sun}(\lambda_D) \cdot RSR_B(\lambda) \cdot BRF_{RSB}^{Prl}(\theta_{in}, \phi_{in}, \lambda) \cdot \Delta BRF_{RSB}(\theta_{in}, \phi_{in}, \lambda, t) d\lambda}{\int RSR_B(\lambda) d\lambda}, \quad (10)$$

In the current SD calibration algorithm, $\Delta BRF_{RSB}(\theta_{in}, \phi_{in}, \lambda, t)$ is assumed to be independent of the incident angles and is replaced by the H-factor, $h(\lambda, t)$, derived from the SDSM calibration under the assumption that the SD degrades uniformly, that is [6],

$$F(B, D, M, G, Scan) = \frac{\tau_{SDS}(\theta_{in}, \phi_{in}) \cdot \cos(\theta_{SD})}{d_{ES}^2 \cdot \sum_{j=0}^{2} c_j(B, D, M, G) \cdot dn_{SD,B}^j(Sample, Scan, D)} \cdot \frac{\int \varepsilon_{Sun}(\lambda_D) \cdot RSR_B(\lambda) \cdot BRF_{RSB}^{Prl}(\theta_{in}, \phi_{in}, \lambda) \cdot h(\lambda, t) d\lambda}{\int RSR_B(\lambda) d\lambda}. \quad (11)$$

It is reasonable assume that $\Delta BRF_{RSB}(\theta_{in}, \phi_{in}, \lambda, t)$ and $h(\lambda, t)$ do not change much with wavelength λ within the narrow bandwidth of the RSB. Then we can write

$$\Delta BRF_{RSB}(\theta_{in}, \phi_{in}, \lambda, t) = \frac{F(B, D, M, G) \cdot h(\lambda, t)}{F(B, D, M, G, Scan)}. \quad (12)$$

The true calibration coefficient or F-factor $F(B,D,M,G)$ only depends on instrument status and should not be angle-dependent. If SD degrades non-uniformly or there is any error in the prelaunch BRF or the SDS VF, then $F(B,D,M,G,Scan)$ may become scan or the incident angle dependent, similar to the H-Factors derived from the SDSM calibration. The errors in the

prelaunch SD BRF and the SDS VF will result in a yearly fluctuation pattern for the variation of the *F(B,D,M,G,Scan)* with respect to the incident angles or the scans, but this pattern does not change beyond the yearly repetition. A trend beyond the annually repeating pattern thus indicates the existence of the effect from non-uniformity in SD degradation. Form Eq. (12), it is seen that the dependence of the scan-dependent F-factors is inversely proportional to the angle-dependence of the SD degradation, which is different from that of the H-factors described in Eq. (6).

As in the BRF_{SDSM} case described in the previous sub-section, to examine the full dependence of BRF_{RTA} on time and angle, we parameterize the scan dependent F-factors as follows [6]

$$F(B,D,M,G,Scan) = a'(\lambda,t)\left[1+b'(\lambda,t)(\phi_{in}-\phi_0)\right], \qquad (13)$$

where *Scan* and declination angle ϕ_{in} has a one-to-one corresponding relationship and ϕ_0 is the reference angle which is the same as that in Eq. (7). The parameter $a'(\lambda,t)$ and $b'(\lambda,t)$ are different characterization parameters from the previous set $a(\lambda,t)$ and $b(\lambda,t)$ in the SDSM case. From Eqs. (12) and (13) one can further work out the following

$$\Delta BRF_{RSB}(\theta_{in},\phi_{in},\lambda_D,t) = a''(\lambda,t)\left[1-b'(\lambda,t)(\phi_{in}-\phi_0)\right]. \qquad (14)$$

Comparing Eqs. (13) and (14), it is seen that the slopes of the scan-dependent F-factors and the SD degradation are opposite as expected and explained previously.

For MODIS, its RSB calibration coefficient is referred to as m1-coefficient and a linear algorithm is applied to relate the radiance and the background subtracted instrument response. The formulation for the SD degradation non-uniformity analysis using the RSB SD observations for MODIS RSB is effectively identical to that for VIIRS RSB and will not be repeated here.

The choice of the instrument coordinate system and the solar declination angle warrants a clarification. As previously mentioned, one can choose any two independent angles in any

coordinate system since one system can always be transformed to another. However, to demonstrate non-uniformity in SD degradation with respect to the incident direction, we have to show that the partial derivative of either one of the two ΔBRFs, $\Delta BRF_{RSB}(\theta_{in},\phi_{in},\lambda,t)$ and $\Delta BRF_{SDSM}(\theta_{in},\phi_{in},\lambda,t)$, with respect to at least one of the two independent angles is not zero and that the derivative also changes with time, as discussed above. Since the SD degrades with time, to obtain the partial derivatives of the either BRF from the SD/SDSM measurements, one is restricted to the data within an event, within which the change of the two BRFs due to the SD degradation should be negligible. In one event of an SD/SDSM measurement, the movement of the satellite results in a smooth change of the declination angle and an almost constant azimuth angle in the instrument coordinate system. In other words, only the partial derivatives of either BRF with respect to the declination angle from the SD/SDSM measurements can be derived and then thus it is the proper and the natural choice in this analysis to use the declination and azimuth angles in instrument coordinate system. Other coordinate systems, such as the SD coordinate system, actually make the analysis more difficult although the final results should be the same if properly done.

3. VIIRS Data Analysis and Results

We present results from both the SDSM and the RSB analysis for SNPP VIIRS. Each scan of an SDSM or RSB calibration measurement, corresponding to an unique incident angle in the range of the sweet spot, is analyzed to reveal the angular dependence in the parameterization $b(\lambda,t)$ or $b'(\lambda,t)$. The examination over the entire history of events then reveals how the angular dependence evolves with respect to time, thus illustrating the effect from SD degradation non-uniformity. This analysis procedure will be identically applied for all sensors in this work.

A. SDSM

The background-subtracted signal of SDSM detector 1 to the SD view for the calibration

event on January 1, 2014, is shown in Fig. 6 as a typical example. The response is plotted against solar declination and the two vertical dash lines mark the sweet spot range between 13° and 17° where scans are fully illuminated and are proper for the calculation of the SD degradation, or H-factor. Figure 7 shows the degradation trend of the H-factor over the first four years as measured by the SDSM at the wavelengths of its 8 detectors [10]. Each point corresponds to one event based on an average of the scans. The SDSM has been established to be an accurate monitor of the SD degradation in the SDSM view direction. The result is smooth and stable, although some unexpected oscillatory feature can be observed starting 2014. The band or spectral dependence is very apparent, with shorter wavelengths going through greater degradation. A recent study has investigated this spectral dependence of the SD degradation utilizing a physical model with the assumption of the SD degradation uniformity [33]. It is shown that the model can well explain the spectral dependence of the SD degradation but it did not provide an assessment of the accuracy in the measured SD degradation. It also did not provide any information concerning the non-uniformity of the SD degradation due simply to its starting assumption on uniform reflectance. Since the reflectance of the SD undergoes greater degradation at shorter wavelengths, we will first demonstrate the SD degradation non-uniformity effect for SDSM detector 1 (412 nm) which exhibits the greatest degradation.

Within the fully illuminated sweet spot for each calibration event there are about 40 available scans, and the 13° to 17° solar declination angle range contains 12 or 13 scans of the SD view that are available for SD degradation calculation. Figure 8 shows the SD degradation at the wavelength of the SDSM detector 1, calculated from Eq. (6), for every available scan for four selected SDSM measurement events – November 15, 2011, March 15, 2012, July 15, 2012 and July 15, 2013. Each H-factor in each event based on the single-scan calculation corresponds to a unique solar declination. The measured data for each event are fitted to a linear regression and then both the data and the fits are normalized to the fitted value at 13° solar declination. The

linear dependence of the SD degradation with respect to solar declination is clearly exhibited for all events, and that the dependence tilts toward greater slope in subsequent events. The slope on November 15, 2011 is about -0.00035 per degree solar declination but on July 15, 2014 event it has grown to 0.00100. This proves that the degradation of the SD is not uniform with respect to incident angles. As the SD degrades, the reflectance at different angles changes at different rates.

Figure 9 shows the history of the evolving angular dependency for all 8 SDSM detectors. The trend for detector 1 exhibits the strongest evolution from being slightly negative to up to 0.001, as discussed above. Except for detector 8 that shows no clear evolution, all other detectors show that the dependence of the response with respect to solar declination progresses positively. In addition, the order exhibited by the 8 wavelengths illustrates wavelength dependence – the shorter the wavelength the greater the effect from SD degradation non-uniformity. For data coming from the SDSM, the degree of the SD degradation non-uniformity effect positively correlates with the degree of SD degradation.

Together with the SD degradation history in Fig. 7, Fig. 9 helps to tell a more complete story of the calibration data evolution as recorded by the SDSM. While each SD degradation result in Fig. 7 comes from the average of the scan response of the calibration event, each point in Fig. 9 reveals the slope, or the angular dependence, of the scan response of the same event. The cumulative effect of the degradation non-uniformity over the sweet spot angular range at wavelength 412 nm can be estimated from Figs. 8 and 9 to be about 0.5% difference over 4° angular range through four years of available data.

B. RSB

Figure 10 shows the background-subtracted response of M1 detector 1 (410 nm) to the SD view for the calibration event on January 1, 2014 for both high- and low-gain settings. Same as

in the SDSM case discussed above, the solar declination angle range is 13° to 17° and the vertical dashed lines mark the sweet spot within which the scans are used in the calculation of the scan-averaged RSB calibration coefficient, or F-factor. Figure 11 shows the standard F-factor for band M1 high-gain mirror-side 1 throughout the mission up to date and that each point is an F-factor computed by averaging over all scans in the sweet spot in that event. For this analysis of the RSB data, we instead compute an F-factor for every scan in the sweet spot using Eq. (11), thus generating about 12 or 13 F-factors per calibration event for examination of their variation with respect to solar declination. Symbols in Fig. 12 are the calculated single-scan F-factor of the RSB M1 detector 1 high gain HAM side 1 versus solar declination for the same 4 selected calibration events as that in the SDSM analysis discussed above. The lines are the linear fits to the calculated F-factors and both measured data and the fits are normalized to the fitted value at 13º solar declination. The result shows a linear dependence on solar declination and that the dependence progressively evolves toward being more negative. Thus both the SDSM detectors and the RSB reveal the degradation non-uniformity effect of the SD. Figure 13 shows the temporal trend as seen by M1 detectors to be highly consistent among all 16 detectors but still with discernable offsets and detector-dependence. The detectors have slightly different outgoing angles with respect to the SD and thus the difference from the actual BRF of the SD toward each detector is expected to manifest. In the standard calculation and this analysis, the band-averaged BRF is used for all detectors and thus the very slight mismatch to each detector generates the offset exhibited in the plot. In principle, the methodology can adapt a detector-dependent BRF to improve this offset among detectors. Another very interesting behavior is the apparent "*turn-off"* or *"turning*" occurring at early 2013 after which the evolution follows a markedly different trend, and is in this case nearly flat. Again the same as in the case for the SDSM, the slopes of the RSB F-factors as shown in Fig. 13 provide a more complete picture of the calibration data evolution, complementing information from Fig. 11 that shows the averaged result of the scans.

Figure 14 shows the trend of the degradation non-uniformity for M1 through M7 (410 to 862 nm), and for detector 8. The result shows clear band-dependence trend just as in the SDSM case in Fig. 9. While it is obvious that shorter wavelengths exhibit greater effect, the four shortest wavelengths (M1–M4, 410 to 551 nm) as a group show distinctively strong evolution until about mid-2013 after which the trend quickly flattens. The physical cause behind this "*turn-off*" phenomenon is not known, but wavelength dependence seems apparent that the shorter wavelengths have earlier *turn-off* or *turning*.

The very small yearly oscillatory pattern is already observable from the start of the mission in Figs. 13 and 14, and indeed is expected as the manifestation of the residual error in BRF and VF of the SDS, for which the dependence on viewing geometry follows a yearly cycle. However, another interesting and key behavior shown in these figures, although not as clear as the MODIS result to be shown later, is the apparent multi-year growth of the yearly oscillation magnitude with respect to time. This is likely another manifestation of the degradation non-uniformity effect and an explanation is provided in the next section.

C. Discussion

The analysis and results described above show that SD degradation is not uniform with respect to incident angles, but the same conclusion can be immediately extended for outgoing angle dependence. By the principle of *optical reciprocity* [34] it can be concluded that from the changing dependence of the instrument response with respect to the incident angle, as demonstrated for the small angle range of the sweet spot, the response will also change for the outgoing angles over the same angle range with respect to the SD normal. The generalization, then, is that the BRDF does not degrade uniformly with respect to the incident and the outgoing angles.

Overall the results clearly demonstrate the effect from SD degradation non-uniformity

through the evolution of the angular dependence is not of the yearly cyclic pattern. The change is particularly intense in the first two years that shows a steep linear drop. For SNPP VIIRS, which is without an SD door but with a permanent screen, the associated degradation non-uniformity effect due to solar exposure is evident. In fact, the apparent increasing yearly fluctuation pattern as mentioned above is another manifestation of the effect. This very likely comes from the effect being shown at different solar azimuth angles that are seasonally varying but yearly repeating. Our analysis captures the effect along the one direction characterized by solar declination but the BRDF as well as the effect are fully two-dimensional phenomena also with dependence on solar azimuth. The calibration events take place at different solar azimuth angles following the yearly orbit around the Sun, and thus the effect over different solar azimuth angles will also manifest as a yearly repeating pattern. However, one major difference is that, while the yearly pattern from the BRF or VF residual error is presumed to identically repeat every year, the trend for the SD degradation non-uniformity effect with respect to solar azimuth angle will increase, in a similar way shown with respect to the solar declination, as the effect accumulates. Interestingly, the residual error due to imperfect BRF or VF characterization furnishes a mean, although indirect, to display the two-dimensional nature of the SD degradation non-uniformity effect through fluctuation magnitude change. While the evolution of the angular dependence along solar declination is directly shown in the underlying trend, the evolution along solar azimuth is exhibited through the growing yearly oscillation.

Figure 15 combines trend results from both the SDSM and the RSB results. For example, lines in red show the SDSM D1 (412 nm) H-factor in dashed line and the corresponding RSB M1 (410 nm) F-factor in solid line. While the F-factor result from the RSB responses analysis may appear to trend differently, since F-factor is inversely proportional to SD degradation, the two sets actually demonstrate vey similar trends. In both cases the incident angle analysis already shows a 0.1% per degree effect over 4 years. Given that the RTA and the SDSM are

separated by more than 100° (see Fig. 16), the discrepancy between the SD degradation factors toward the two respective outgoing directions conceivably can be much more significant, up to ~10% assuming a consistent linear relationship along the declination angle direction in the angular range from the SDSM view direction to that of the RTA. However, this cannot be the real case. In fact, additional azimuthal dependence and different quantitative relationship beyond the analyzed angular range will bring in greater complexity. It is hardly possible to determine the real differences between the SD degradations between the two view directions and further investigation on this issue is beyond the scope of this work. In reality ~1% bias in SNPP VIIRS SD-based calibration results [6, 11, 23] has already been observed against lunar-based calibration [32, 35] and this inaccuracy has seriously impacted ocean color products [36]. Greater details of the mitigation approach via the "Hybrid Methodology" specific to SNPP VIIRS will be provided in the general discussion.

The combine H-factor and F-factor results of Fig. 15 demonstrate once again that the BRF and the VF of the SDS were derived accurately from the planned on-orbit yaw maneuver executed on day 110, February 14 and February 15, 2012. Once the maneuver measurement and the ensuing characterization analysis have correctly captured the BRF angular dependence at day 110, then the slopes from our analysis show the changing angular dependence relative to that result, starting from zero. The same is also shown in Figs. 9 and 13. In all figures, it can be seen that the slopes of the angular dependence are close to zero at that time, showing that the characterization re-analysis indeed correctly captured the angular dependence in the BRF for day 110.

4. MODIS Data Analysis and Results

Analyses and results for the SD degradation non-uniformity effect for MODIS using RSB SD calibration measurements are presented. The main procedure is identical to one previously described for SNPP VIIRS. Within each calibration event every valid scan is used to compute

one scan-based RSB calibration coefficient, or m1 coefficient for MODIS, and a simple linear regression is fitted to the m1 coefficient versus solar declination as described in Eqs. (11)–(13). The fitted slopes are plotted for the mission and examined.

A. Terra MODIS

In comparison with SNPP VIIRS, the SD degradation non-uniformity effect in Terra MODIS is significantly more dramatic. Figure 17 shows the Band 8 (412 nm) trend evolves down to about –0.2%, but the corresponding VIIRS RSB M1 (410 nm) trend in Fig. 13 shows a smaller effect at –0.1%. Its large and noisy yearly oscillation on top of the underlying trend is also very apparent, and it primarily comes from the residual error in its VF of the SDS – this fact that it is the VF and not the BRF in case of MODIS will be discussed later. Figure 18 shows the Band 12 (551 nm) result for its 10 detectors. In comparison with the equivalent VIIRS band M4 (551 nm, see 5-pointed star curve in Fig. 14) the effect in Band 12 is about six times steeper, thus showing that the effect is more serious in Terra MODIS. Since Terra MODIS has undergone the most dramatic degradation, at nearly 40% at the shortest wavelengths, the associated SD degradation non-uniformity effect is expectedly more dramatic. Both Band 8 and Band 12 exhibit the same consistent trend offset among all detectors in the same band, same as previously shown in SNPP VIIRS, due to the slight mismatch between the applied band-averaged BRF and each detector. The *turning* trend change in 2007 with a subsequent weakly lowering trend can also be seen in Band 8, but for Band 12 its turning is later, at 2008. In Fig. 19, Band 8 through Band 12 (412 to 551 nm) detector 6 results show that the effect is strong in Terra MODIS, up to 0.3%, at short wavelengths. The effect appears to be a function of wavelength, e.g., that Band 8 trends lower than Band 12. Turn-off (or turning) is also apparently band-dependent, but a more careful quantification in future investigations will be required to be more definitive.

In all plots, the yearly variation artifact fluctuates strongly, up to 8 times greater in comparison to SNPP VIIRS. This shows that its SDS VF [37], τ_{SDS}, does not describe the transmittance of the screen with good accuracy. The emergence of the strong yearly fluctuations comes primarily from the residual error of the screen VF and not the BRF will be discussed later. The yearly variation of about 0.2% effect from the VF residual is already visible in the first three years prior to the SD door anomaly in 2003 (Figs. 17 and 18), even though the SD degradation non-uniformity effect has not yet become significant. During this early period Terra MODIS calibration events operated as designed and the SD door was kept closed except during calibration events. An SD door operation anomaly occurring in July 2003 led to the decision to keep the SD door in permanent open position and the screen in permanent closed position starting July 2, 2003 [1]. A vertical dashed line in the figure marks this event. It is apparent that the continual excessive solar exposure after the SD door anomaly intensified the effect for the subsequent mid-2003 to mid-2006 period, as demonstrated in the strong down turning trend. While the VF or BRF residual error can induce varying oscillation pattern its magnitude or the underlying trend will not steadily grow beyond the yearly repetition, and thus the observed clear multi-year trend is the evidence of the SD degradation non-uniformity effect. In addition, the magnitude of the oscillation of the yearly VF residual pattern shows steady growth. This is also revealed by SNPP VIIRS, discussed previously, due to the dependence of the effect at different solar azimuthal angles. At about 2007 the trend shows a near *turned off*, a similar sharp behavioral change seen also in SNPP VIIRS. In 2012 another distinctive upward trend shift can be seen. Band 8 in Fig. 17 exhibits one additional and potentially new phenomenon, i.e., some distinctive sudden changes in the magnitude of the yearly oscillation artifact are seen, the most noticeably the change around 2007. Changes are also apparent in 2003 and 2012. This telltale

evidence points to the possibility that the screen has gone through sudden physical changes on-orbit that amplified the residual error. An examination of Figs. 18 and 19 suggests that all five bands, B8 through B12, exhibit this phenomenon. Even though the changes in B11 and B12 are not as distinctive due to the two bands having a weaker oscillation magnitude, the change in 2003 is nevertheless visible.

B. Aqua MODIS

Figure 20 showcases the evolution of the angular dependence for Aqua Band 8 (412 nm) mirror side 1 for the screened case for its 10 detectors. It is immediately noted that the SD degradation non-uniformity effect, embedded within the noisy yearly fluctuation pattern, is at a very gentle level of 0.02% per year through out its mission, and is in fact more mild than the equivalent VIIRS band M1 (410 nm) result at about 0.05% per each of its first two years as seen in Figs. 13 and 14. The SD of Aqua MODIS has had the most gentle degradation among the three sensors, at about 20% overall at 412 nm wavelength. Nevertheless the yearly oscillation artifact due to the VF residual at about 0.2% is also large and comparable to that of Terra MODIS, and is similarly indicative of its VF not being as well-characterized [37]. It will be shown later that the yearly oscillation artifact in Aqua MODIS result comes mainly from the VF residual and not from the BRF. The detectors also demonstrate very consistent offset throughout all 13 years, as already shown for SNPP VIIRS and Terra MODIS coming from the use of the band-averaged BRF.

The B8–B12 (412 to 551 nm) result in Fig. 21 shows a clear band-dependence of the SD degradation non-uniformity effect in that the shorter the wavelength the stronger the effect. B11 and B12 (531 and 551 nm) trends are flat, and this is well compared to the VIIRS M4 (551 nm) result in Fig. 14, which also shows a mild change. We again expect the effect to have

correspondence at the same wavelength between the two sensors but that Aqua MODIS would exhibit lesser effect due to having lesser degradation.

C. Discussions

All previous analysis results are shown for the screened case and thus the impact of residual error from the VF of the SDS, τ_{SDS}, is present in all as yearly fluctuations. However, unlike Terra MODIS for which the SD port remains completely screened after July 2003 or SNPP VIIRS with a permanent fixed screen in front of the SD port, Aqua MODIS calibration operations have included both screened and unscreened measurements that can reveal clear differences between the two cases. We can derive the slopes from the SD measurements for the two cases with and without the SD screen in the front of the SD port. We use Band 3 for this purpose because MODIS Bands 8–16 saturate during an SD calibration with open screen. In Fig. 22, the residual effect of the VF is demonstrated via Aqua MODIS band 3 (469 nm) in the screened case. The yearly pattern fluctuating up to 0.4% is significant as is in the Terra MODIS case. In contrast, Fig. 23 shows the unscreened result that demonstrates a very clean trend with hardly much noise. This proves that the screen vignetting effect and its residual error is the source of the strong yearly fluctuation pattern in Aqua MODIS. In actuality, Terra MODIS prior to the SD door anomaly in 2003 also followed a normal screen and unscreened measurement operations and its results during this early period similarly showed that the screened case has a large yearly fluctuation pattern but that the unscreened case is clean. The impact of the VF residual was not previously discussed for SNPP VIIRS due simply to its much smaller level at ~0.05%, which is nearly an order of magnitude smaller than that from MODIS. The VF and the BRF applied for SNPP VIIRS in this study are the same ones independently and carefully re-derived in the previous works on RSB calibration and mitigation of calibration bias [29].

5. General Discussions

Numerous interesting phenomena have been shown to be common among the three sensors, including the constant offsets among detectors of the same band, the multi-year trend change of the angular dependence showing SD degradation non-uniformity effect, and the yearly fluctuations. Respectively, these are revelations about the SD BRF, the associated SD effect, and the SDS VF, τ_{SDS}. There are also at least two interesting new phenomena uncovered in this dedicated study, not necessarily yet proven to be common for all, that are worthy of further discussion. One is the turning or turn-off of the slope trend – or the sharp change in the angular dependence of the SD degradation non-uniformity – revealed by SNPP VIIRS and Terra MODIS. This suggests the existence of a threshold, at least exhibited along the solar declination direction. However, it does not imply a true or common threshold since behavior along other directions may be different. In addition, the threshold is band or wavelength dependent as demonstrated in Figs. 17–19. In both SNPP VIIRS and Terra MODIS without an SD door in closed position, the SD has been under constant solar exposure or the harsh space environment conditions and thus the effect has strongly evolved to expose some possible additional physical constraint. Aqua MODIS result does not show this behavior, but presumably the cumulative SD degradation non-uniformity effect has been mild and likely not yet sufficient to expose any constraint. In this respect, Aqua MODIS provides very important complementary information, different from SNPP VIIRS and Terra MODIS, when the associated degradation effects are weak. The second phenomenon is the sudden changes in the magnitude of the yearly fluctuations in the Terra MODIS trend as seen in Fig. 17, at early 2003, then 2007 and finally another at 2012. As the yearly pattern is the manifestation of the residual error from VF as discussed in the previous section, this implies a sudden change in the physical property of the SD screen but other alternatives may exist or co-exist. Again the constant solar exposure and the harsh space environment may have had serious impacts on the Terra MODIS SD screen after

many years on orbit. Since SNPP VIIRS is without an SD door, its SD screen faces the same constant solar exposure and the harsh space environment. Currently, no sudden changes are seen in the magnitude of the yearly oscillation for VIIRS. Given that VIIRS has only been on orbit for a comparably short time, it may take a few more years before the physical change of the SD screen can occur. For Aqua MODIS, an operational SD door has well protected its SD screen and this is shown in the very steady yearly oscillation pattern from the VF residual in Figs. 20 and 21. This result is consistent with its SD screen not having gone through any physical change.

For SNPP VIIRS, the SD-based calibration bias has already been observed to grow up to ~1% against lunar-based calibration in the past few years. The ocean color products in particular, being very sensitive to sensor data, have been seriously impacted by the calibration inaccuracy. Investigations by Sun and Wang [11] identified the SD degradation effect and led to a mitigation "Hybrid Methodology" strategy that combines lunar-based and SD-based calibration to fix the SD calibration bias induced by the effect and/or other possible errors. The VIIRS instrument layout places the SV, through which lunar observations are made, at the same angle of incidence (AOI) as the SD view. This design element thus enables the direct comparison between the SD-based and the lunar-based calibration results, by averting the RVS effect of the scan mirror, and permits a straightforward combination of the two results to generate hybrid RSB calibration coefficients that accurately describe the on-orbit changes of the SNPP VIIRS RSB. The significant improvement in the re-derived ocean color products, for example in showing very good agreement with the in situ data [11, 23, 36], validates the correctness of the hybrid calibration coefficients and that the SD-based calibration inaccuracy indeed caused the long-term drift seen in VIIRS ocean color products. For MODIS, the SV and the SD view have very different AOIs and thus the direct lunar versus SD comparison cannot be used due to the AOI dependence of the RVS on-orbit change of the scan mirror even though the lunar calibration

accurately tracks the gain changes at AOI of the SV [38]. Consequently, the mitigation scheme similar to the SNPP VIIRS hybrid methodology cannot be applied to MODIS instruments. Prior to L1B Collection 6, the SD calibration error in Terra MODIS was revealed to be as high as ~10% in Band 8 (412 nm) through comparison with earth targets analysis although reasons were unknown and certainly the errors may not be completely induced by the SD degradation uniformity effect. Aqua MODIS SD calibration inaccuracy was at a more modest scale, for example in Band 8 the error was only about 1% or less [24, 25]. In either case, the earth targets analysis on Terra and Aqua MODIS already hinted a connection between the calibration bias and the associated degradation effects. The success of the desert targets analysis enabled *Sun et al.* [24, 25] to adopt the use of earth desert targets in the development of MODIS C6 methodology to resolve the accuracy issue of both the time-dependent RVS and the SD-based calibration coefficients. The MODIS C6 approach simply abandons the SD-based and older approaches for bands that exhibit SD-based calibration and RVS characterization failures and opted for an entirely different calibration source [24, 25]. However, one important caveat of MODIS C6 is that, while the methodology is a full and robust characterization scheme, each earth target update requires proper and careful treatments. Since earth target data are inherently noisier than the required accuracy, the details of the treatments such as in proper fittings are crucial in generating optimal results. At the time of its initial completion, MODIS Collection 6 has adopted earth-based calibration for Terra MODIS bands 3, 8, 9 and 10 and for Aqua MODIS bands 8 and 9, the affected short-wavelength bands [24, 25].

Although Aqua MODIS has been operating on orbit for 13 years, its SD has degraded less than that of SNPP VIIRS, which has been operating only for slightly more than four years. In the order of overall SD degradation, Terra MODIS is at ~40%, SNPP VIIRS is at ~30%, and Aqua MODIS is at ~20% [10, 13]. This is in accord with the known SD accuracy bias of Terra MODIS at ~10%, SNPP VIIRS at ~1%, and Aqua MODIS at less than 1% [11, 24, 25]. Our

analysis reveals the degree of the SD degradation non-uniformity effect to follow the same order, indicating that the effect directly correlates to the overall SD reflectance performance degradation. However, although we have illuminated a connection, no clear quantitative or analytical relationship between the effect and radiometric calibration bias can be claimed, and further investigations for progress in this direction are required. From the perspective of achieving long-term robustness of the calibration, the best operational practice is to close the port door to minimize SD degradation and to reduce calibration bias coming from the associated degradation non-uniformity effect that escapes the standard calibration procedure. It also reduces the solar and space environmental impact on the SD screen as discussed previously, thus preventing the possible change of VF. Currently, the SNPP VIIRS SD degradation is on pace to match Terra MODIS, and certainly with continuing solar exposure its calibration bias due to SD degradation non-uniformity effect is expected to worsen further. *As the current VIIRS design is without an SD door, future VIIRS missions may consider redesigning to include an SD door and formulating a new operation schedule similar to Aqua MODIS*. The concrete and the significant benefits to be gained, namely achieving highly accurate calibration result, can be important factors to be weighted against cost and risks, which includes the SD door anomaly that happened for Terra MODIS in 2007. We further point out that the success of "Hybrid Methodology" for SNPP VIIRS is due to a cross-disciplinary understanding of sensor calibration and instrument layout and design.

Lastly, we make a suggestion that a set of late mission on-orbit yaw maneuvers would be a worthy consideration that can yield valuable insights, most importantly on the so called BVP, the product of SD BRF and VF, which is the first of key inputs for RSB calibration [29, 30]. For twin MODIS, which are near their end-of-mission after having served more than twice the intended lifetime, this would be a particularly timely discussion. The new yaw measurement can be compared with the earlier yaw result for a direct check of the changing SD property on-orbit,

especially the non-uniformity in SD degradation with respect to the incident and outgoing directions. As mentioned previously, evidence from MODIS results also points to physical changes of the screen, and end-of-mission yaw maneuvers can shed more light on this new phenomenon. The new information would be of great interest to the calibration community, engineers and vendors alike. As there will be more VIIRS follow-up missions, namely J1 through J4 VIIRS, ample opportunities exist for end-of-mission yaw maneuvers to collect a wealth of information on the SD and their BRF or VF. For RSB calibration that continues to rely on the SD at its core, this information and the ensuing analyses can be of tremendous benefits in improving SD designs and calibration methodology and achieving accurate and long-term science results.

6. Conclusions

The degradation non-uniformity in the bi-directional reflectance distribution function of the solar diffuser has been demonstrated to be a general phenomenon occurring on-orbit. The evidence from the calibration data history from three sensors paints a clear picture that as the reflectance of the solar diffuser degrades, its angular dependence is also altered. The visible bands show the most pronounced effect, but two near-infrared bands in VIIRS, M7 and M8 bands, also show weak but observable effect. The degradation non-uniformity effect impacts the solar diffuser-based RSB calibration methodology due to the buildup of the discrepancy between the degradation factor measured by the SDSM and the one viewed by the RSB, and eventually long-term bias is manifested in associated derived science products. This investigation strengthens our previous investigations on SNPP VIIRS calibration, and additionally helps to identify and clarify for MODIS one primary source of error in RSB calibration and the associated science products that motivated the MODIS Collection 6 methodology. Nevertheless successful mitigations have also been pointed out for both MODIS and VIIRS, and it

demonstrates that with proper design and understanding of calibration, the employment of solar diffuser continues to have merits. While our exposition is successful in the intended study, it reveals more previously unknown phenomena, such as the sharp behavioral change in the SD degradation non-uniformity and the possible sudden physical change of the SD screen, and certainly these phenomena can be appropriate topics for future studies. Among the many lessons learned, one particularly relevant is that minimizing the solar diffuser degradation and associated effects could be a key factor for long-term sustainable and reliable science output. This purpose can be well served by having the capability of the solar diffuser door open-close operationally.

ACKNOWLEDGEMENTS

The work was supported by the Joint Polar Satellite System (JPSS) funding. We thank Jennifer Dodd for her valuable comments and suggestions. The views, opinions, and findings contained in this paper are those of the authors and should not be construed as an official NOAA or U.S. Government position, policy, or decision.

REFERENCES

1. X. Xiong, J. Sun, W. Barnes, V. Salomonson, J. Esposito, H. Erives, and B. Guenther, "Multi-year On-orbit Calibration and Performance of Terra MODIS Reflective Solar Bands," *IEEE Trans. Geosci. Remote Sens*., 45, 879-889 (2007).
2. X. Xiong, J. Sun, X. Xie, W. Barnes, and V. Salomonson, "On-Orbit Calibration and Performance of Aqua MODIS Reflective Solar Bands," *IEEE Trans. Geosci. Remote Sens.*, 48, 535-546 (2010).
3. R. E. Eplee, F. S. Patt, R. A. Barnes, and C. R. McClain, "SeaWiFS long-term solar diffuser reflectance and sensor noise analyses," *Appl. Opt*., 46, 762-773 (2007).

4. J. C. Cardema, K. Rausch, N. Lei, D. I. Moyer, and F. DeLuccia, "Operational calibration of VIIRS reflective solar band sensor data records," Proc. SPIE, 8510, 851019 (2012).
5. X. Xiong, J. Butler, K. Cjiang, B. Efremova, J. Fulbright, N. Lei, J. Mclntire, H. Oudrari, J. Sun, Z. Wang, and A. Wu, "VIIRS on-orbit calibration methodology and performance", *J. Geophys. Res. Atmos.*, 119, 5065–5078 *(2014).*
6. J. Sun and M. Wang, "On-orbit calibration of Visible Infrared Imaging Radiometer Suite reflective solar bands and its challenges using a solar diffuser," *Appl. Opt.*, 54, 7210-7223 (2015).
7. R. E. Eplee, Jr., K. R. Turpie, G. Meister, F. S. Patt, B. A. Franz, S. W. Bailey, "On-orbit calibration of the Suomi National Polar-Orbiting Partnership Visible Infrared Imaging Radiometer Suite for ocean color applications," *Appl. Opt.* 54, 1984-2006 (2015).
8. N. Lei, Z. Wang, and X. Xiong, "On-Orbit Radiometric Calibration of Suomi NPP VIIRS Reflective Solar Bands Through Observations of a Sunlit Solar Diffuser Panel,"*IEEE Trans. Geosci. Remote Sens.*, 53, 5983-5990 (2015).
9. C. J. Bruegge, A. E. Stiegman, R. A. Rainen, A. W. Springsteen, "Use of Spectralon as a diffuse reflectance standard for in-flight calibration of earth-orbiting sensors", *Optical Engineering*, 32, 805-814 (1993).
10. J. Sun and M. Wang, "Visible infrared image radiometer suite solar diffuser calibration and its challenges using solar diffuser stability monitor," *Appl. Opt*., 53, 8571-8584 (2014).
11. J. Sun and M. Wang, "Radiometric calibration of the Visible Infrared Imaging Radiometer Suite reflective solar bands with robust characterizations and hybrid calibration coefficients", *Appl. Opt*., 54, 9331-9342 (2015).
12. E. Grossman and I. Gouzman, "Space environment effects on polymers in low earth orbit", *Nucl. Instrum. Methods, Phys. Res. Sect. B, Beam Interact. Mater. Atoms*, 208, 48-57 (2012).
13. X. Xiong, A. Angal, J. Sun, T. Choi, and E. Johnson, "On-orbit performance of MODIS solar diffuser stability monitor", Journal of Applied Remote Sensing, 8, 083514-1-14 (2014).

14. E. Hass, D. Moyer, F. DeLuccia, K. Rausch, and J. Fulbright, "VIIRS solar diffuser bidirectional reflectance distribution function (BRDF) degradation factor operational trending and update," Proc. SPIE, 8510, 851016 (2012).
15. J. Fulbright, N. Lei, K. Chiang, and X. Xiong, "Characterization and performance of the Suomi-NPP VIIRS solar diffuser stability monitor," Proc. SPIE, 8510, 851015 (2014).
16. H. R. Gordon and M. Wang, "Retrieval of water-leaving radiance and aerosol optical thickness over the oceans with SeaWiFS: A preliminary algorithm," *Appl. Opt.* 33, 443–452 (1994).
17. M. Wang, "Remote sensing of the ocean contributions from ultraviolet to near-infrared using the shortwave infrared bands: simulations," *Appl. Opt.* 46, 1535–1547 (2007).
18. M. Wang and W. Shi, "The NIR-SWIR combined atmospheric correction approach for MODIS ocean color data processing," *Opt. Express*,15, 15722–15733 (2007).
19. M. Wang, J. Tang, and W. Shi, "MODIS-derived ocean color products along the China east coastal region," *Geophys. Res. Lett.* 34, L06611 (2007).
20. M. Wang, W. Shi, and J. Tang, "Water property monitoring and assessment for China's inland Lake Taihu from MODIS-Aqua measurements," *Remote Sens. Environ.*, 115, 841–854 (2011).
21. M. Wang, X. Liu, L. Tan, L. Jiang, S. Son, W. Shi, K. Rausch, and K. Voss, "Impact of VIIRS SDR performance on ocean color products," *J. Geophys. Res. Atmos.* 118, 10347–10360 (2013).
22. M. Wang, X. Liu, L. Jiang, S. Son, J. Sun, W. Shi, L. Tan, P. Naik, K. Mikelsons, X. Wang, and V. Lance, "Evaluation of VIIRS ocean color products," *Proc. SPIE*, 9261, 92610E (2014).
23. J. Sun and M. Wang, "VIIRS Reflective Solar Bands Calibration Progress and Its Impact on Ocean Color Products," *Remote Sensing*, 8, 194, (2016).

24. J. Sun, X. Xiong, A. Angal, H. Chen, A. Wu, and X. Geng, “Time dependent response versus scan angle for MODIS reflective solar bands,” *IEEE Trans. Geosci. Remote Sens.*, 52, 3159-3174 (2014).
25. J. Sun, A. Angal, X. Xiong, H. Chen, X. Geng, A. Wu, T. Choi, and M. Chu, “MODIS RSB calibration improvements in Collection 6,” *Proc. SPIE*, 8528, 85289N (2012).
26. J. Sun and X. Xiong, "Solar and lunar observation planning for Earth-observing sensor", *Proc. SPIE*, 8176, 817610 (2011).
27. J. Butler, X. Xiong, R. A. Barnes, F. S. Patt, J. Sun, and K. Chiang, “An overview of Suomi NPP VIIRS calibration maneuvers,” *Proc. SPIE,* 8510, 85101J (2012).
28. X. Xiong, J. Sun, J. Esposito, X. Liu, W. Barnes, and B. Guenther, “On-orbit characterization of a solar diffuser’s bidirectional reflectance factor using spacecraft maneuvers,” *Proc. SPIE*, 5151, 375-383 (2003).
29. J. Sun and M. Wang, “On-orbit characterization of the VIIRS solar diffuser and solar diffuser screen," Appl. Opt., 54, 236-252 (2015).
30. J. McIntire, D. Moyer, B. Efremova, H. Oudrari, X. Xiaoxiong, “On-Orbit Characterization of S-NPP VIIRS Transmission Functions”, *IEEE Trans. Geosci. Remote Sensing* 53, 2354 - 2365 (2015).
31. C. Cao, F. Deluccia, X. Xiong, R. Wolfe, and F. Weng, “Early on-orbit performance of the Visible Infrared Imaging Radiometer Suite (VIIRS) onboard the Suomi National Polar-orbiting Partnership (S-NPP) satellite,” IEEE Trans. Geosci. Remote Sens., 52, 1142–1156 (2014).
32. J. Sun, X. Xiong, and J. Butler, “NPP VIIRS on-orbit calibration and characterization using the Moon,” *Proc. SPIE*, vol. vol. 8510, pp. 85101I (2012).
33. X. Shao, C. Cao, T.-C. Liu, ”Spectral Dependent Degradation of the Solar Diffuser on Suomi-NPP VIIRS Due to Surface Roughness-Induced Rayleigh Scattering,” *Remote Sens.*, 8, 254 (2016). doi: 10.3390/rs8030254.

34. M. Born and E. Wolf, “Principles of Optics: Electromagnetic theory of propagation, interference and diffraction of light”, 7th edition, Cambridge Press, p423 (1999).
35. X. Xiong, J. Sun, J. Fulbright, Z. Wang, and J. Butler, “Lunar Calibration and Performance for S-NPP VIIRS Reflective Solar Bands”, submitted to *IEEE Trans. Geosci. Remote Sensing.*, 54, 1052-1061 (2016).
36. M. Wang, X. Liu, L. Jiang, S. Son, J. Sun, W. Shi, L. Tan, P. Naik, K. Mikelsons, X. Wang, V. Lance, “VIIRS ocean color research and application,” *Proc. The IEEE International Geoscience and Remote Sensing Symposium (IGARSS)*, 2911-2914, Milan, Italy (2015). doi: 10.1109/IGARSS.2015.7326424.
37. X. Xie, X. Xiong, D. Moyer, J. Sun, X. Liu, and W. Barnes, **“**Analysis of MODIS solar diffuser screen vignetting function, Earth Observing Systems X**,”** *Proc. SPIE*, 5882, 58820T (2005).
38. J. Sun, X. Xiong, W. L. Barnes, and B. Guenther, “MODIS Reflective Solar Bands On-Orbit Lunar Calibration”, *IEEE Trans. Geosci. Remote Sens*. 43, 2383-2393 (2007).

FIGURE CAPTIONS

Figure 1. VIIRS solar diffuser.

Figure 2. SNPP VIIRS layout.

Figure 3. A schematic of SD/SDSM calibration.

Figure 4. Schematic of on-orbit SD/SDSM calibration event.

Figure 5. Solar angles in the instrument coordinate system.

Figure 6. Background-subtracted response of SNPP VIIRS SDSM detector 1 to the SD view on January 1, 2014.

Figure 7. SNPP VIIRS SD degradation.

Figure 8. Symbols are VIIRS SD degradation at wavelength 412 nm calculated by Eq. (6) from the measurements of the SDSM detector 1. Each symbol corresponds to one scan. Solid lines are linear functions fitted to the corrected dc. All data for each event are normalized to the linear function of the event at declination angle 13^{o}.

Figure 9. Slopes of the normalized fitted linear function from SDSM of SNPP VIIRS. Non-dependence with respect to solar declination angle should result in flat trends.

Figure 10. Background subtracted response of SNPP VIIRS band M1 detector 1 when it viewed SD on January 1, 2014 and the "sweet spot" for the RSBs viewing the SD.

Figure 11. SNPP VIIRS band M1 high gain HAM side 1 calibration coefficients.

Figure 12. Symbols are F-factors of band M1 detector 8 high gain HAM side 1 for SD view, calculated by Eq. (4). Each symbol corresponds to one scan. Solid lines are linear functions fitted to the F-factors. All data for each event are normalized to the linear function of the event at declination angle of 13^{o}.

Figure 13. Slopes of the normalized fitted linear functions for SNPP VIIRS Band M1 high gain HAM side 1.

Figure 14. Slopes of the normalized fitted linear functions for all RSB detector 8 high gain HAM side 1.

Table 1. VIIRS and MODIS Specification

VIIRS SDSM		VIIRS RSB			MODIS RSB	
Detector	CW* (nm)	Band	CW* (nm)	Gain	Band	CW*(nm)
D1	412	M1	410	DG	B8	412
D2	450	M2	443	DG	B9	443
NA	NA	NA	NA	NA	B3	469
D3	488	M3	486	DG	B10	488
NA	NA	NA	NA	NA	B11	531
D4	555	M4	551	DG	B12	551
D4	555	M4	551	DG	B4	555
NA	NA	I1	640	SG	B1	645
D5	672	M5	671	DG	B13	667
D5	672	M5	671	DG	B14	678
D6	746	M6	745	SG	B15	748
NA	NA	NA	NA	NA	B2	858
D7	865	M7	862	DG	B16	869
D7	865	I2	862	SG	B16	869
NA	NA	NA	NA	NA	B17	905
D8	935	NA	NA	NA	B18	936
D8	935	NA	NA	NA	B19	940
NA	NA	M8	1238	SG	B5	1240
NA	NA	M9	1378	SG	B26	1375
NA	NA	M10	1610	SG	B6	1640
NA	NA	I3	1610	SG	B6	1640
NA	NA	M11	2250	SG	B7	2130
*CW: Center Wavelength; DG: Dual Gain; SG: Single Gain						

Figure 1. VIIRS solar diffuser.

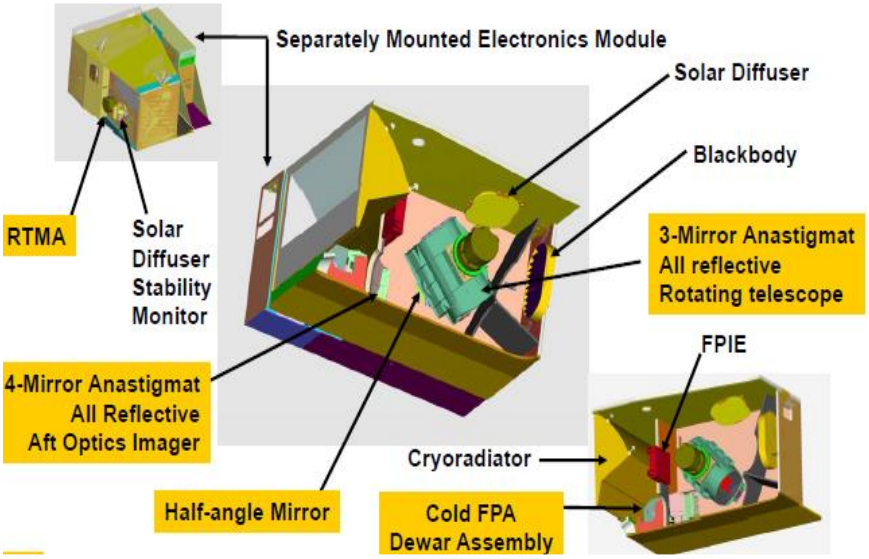

Figure 2. SNPP VIIRS layout.

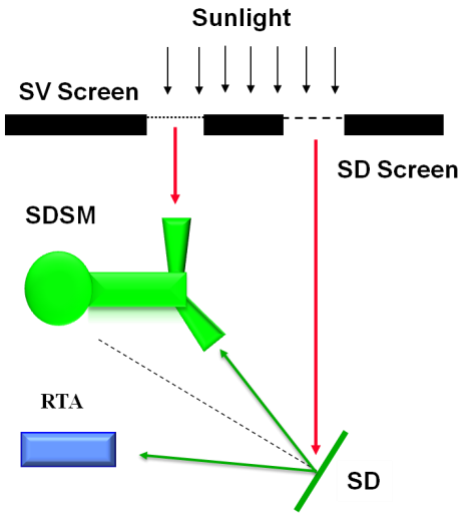

Figure 3. A schematic of SD/SDSM calibration.

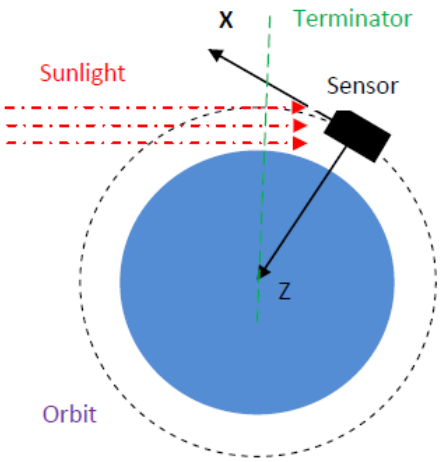

Figure 4. Schematic of on-orbit SD/SDSM calibration event.

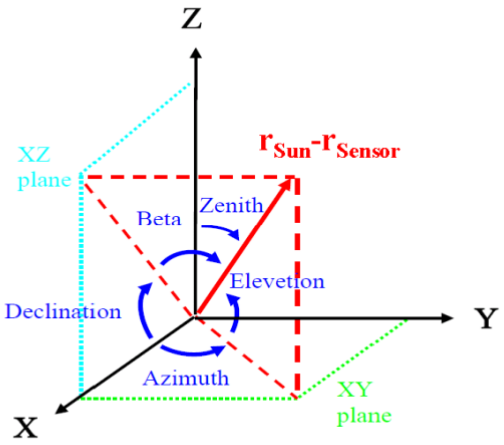

Figure 5. Solar angles in the instrument coordinate system.

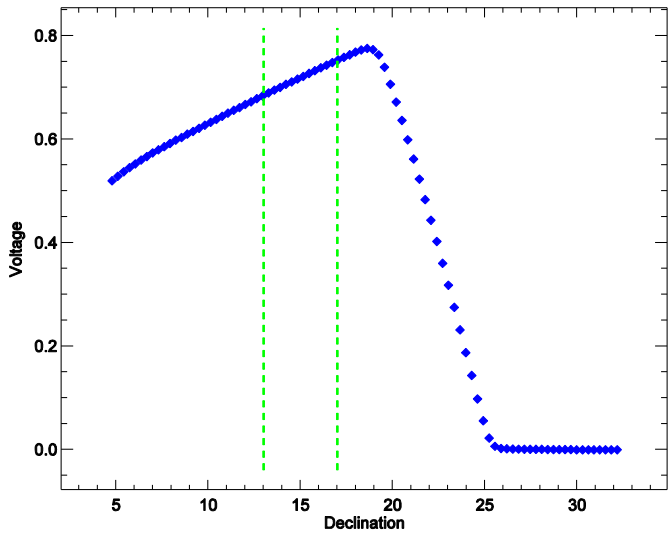

Figure 6. Background-subtracted response of SNPP VIIRS SDSM detector 1 to the SD view on January 1, 2014.

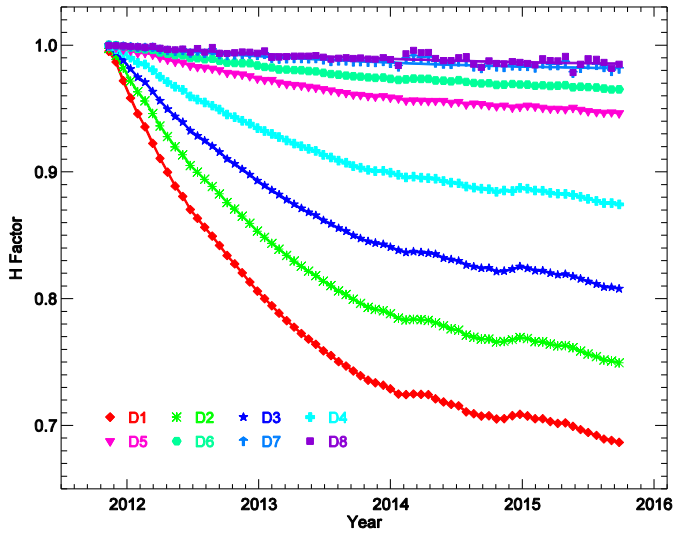

Fig. 7. SNPP VIIRS SD degradation.

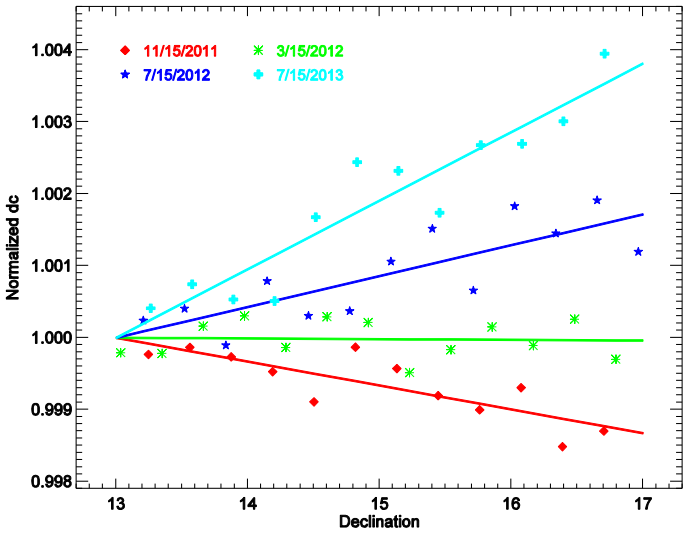

Figure 8. Symbols are VIIRS SD degradation at wavelength 412 nm calculated by Eq. (6) from the measurements of the SDSM detector 1. Each symbol corresponds to one scan. Solid lines are linear functions fitted to the corrected dc. All data for each event are normalized to the linear function of the event at declination angle 13^{o}.

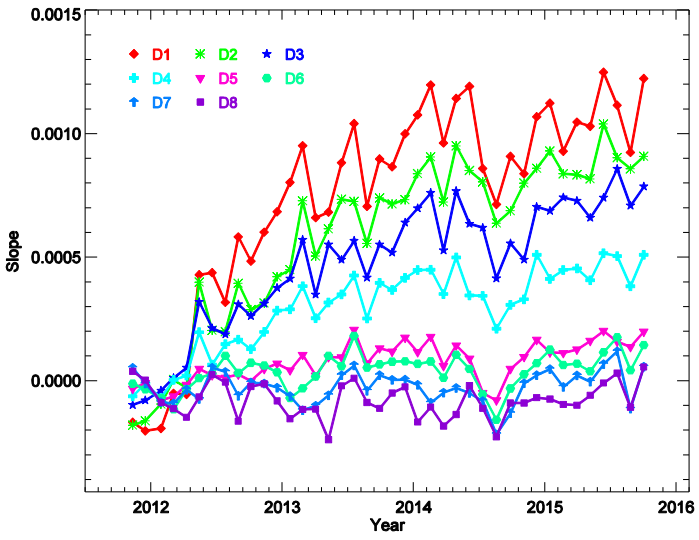

Figure 9. Slopes of the normalized fitted linear function from SDSM of SNPP VIIRS. Non-dependence with respect to solar declination angle should result in flat trends.

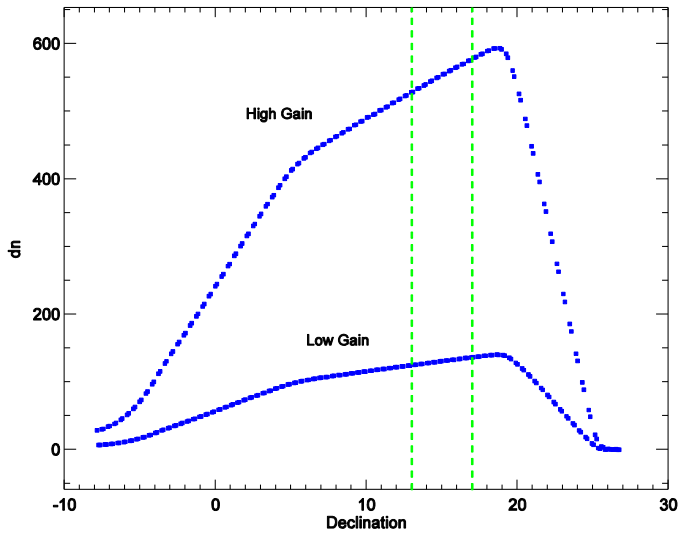

Figure 10. Background subtracted response of SNPP VIIRS band M1 detector 1 when it viewed SD on January 1, 2014 and the "sweet spot" for the RSBs viewing the SD.

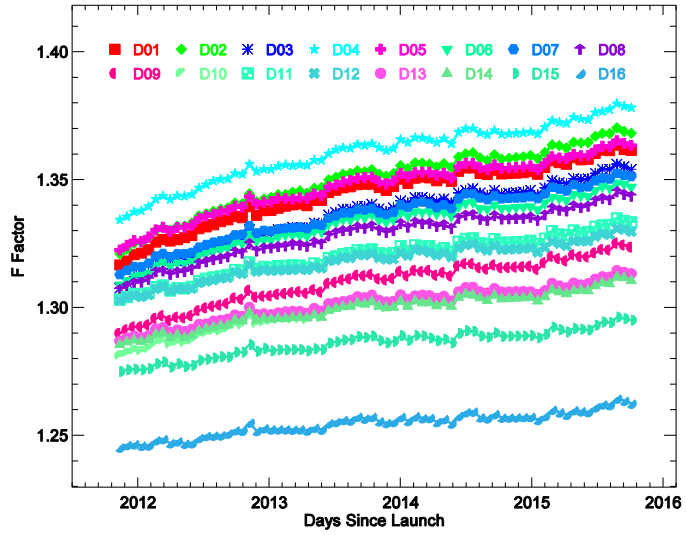

Figure 11. SNPP VIIRS band M1 high gain HAM side 1 calibration coefficients.

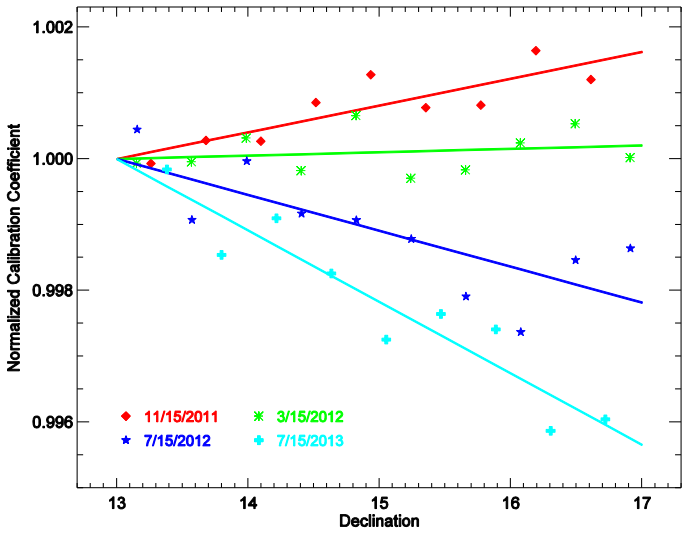

Figure 12. Symbols are F-factors of band M1 detector 8 high gain HAM side 1 for SD view, calculated by Eq. (4). Each symbol corresponds to one scan. Solid lines are linear functions fitted to the F-factors. All data for each event are normalized to the linear function of the event at declination angle of 13^{o}.

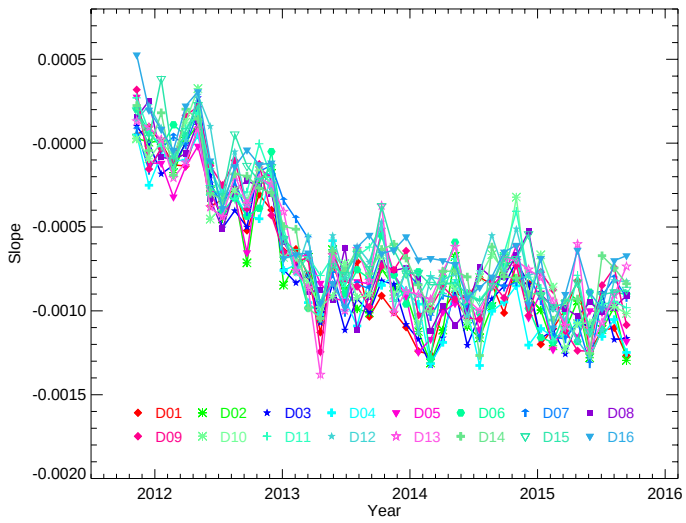

Figure 13. Slopes of the normalized fitted linear functions for SNPP VIIRS Band M1 high gain HAM side 1.

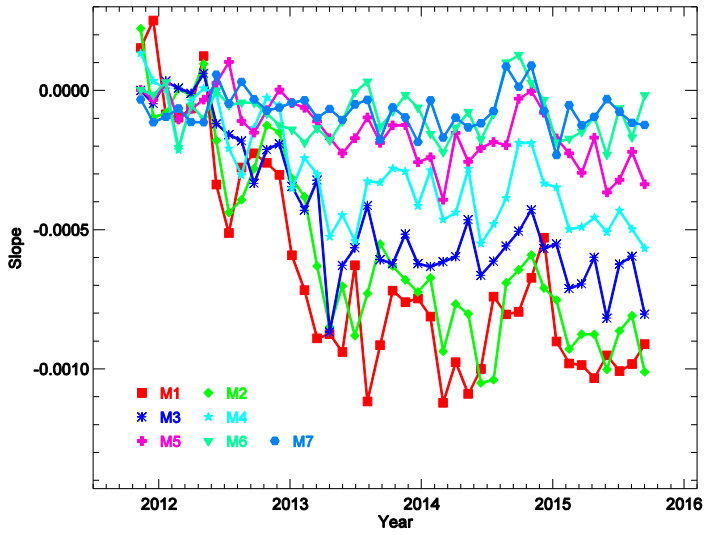

Figure 14. Slopes of the normalized fitted linear functions for all RSB detector 8 high gain HAM side 1.

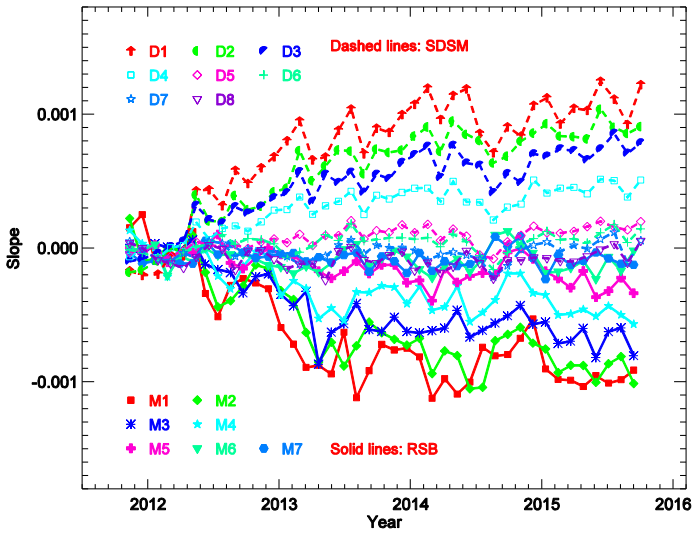

Figure 15. Slopes of H-factors and F-factors (detector 8) in each individual event with respect to solar declination.

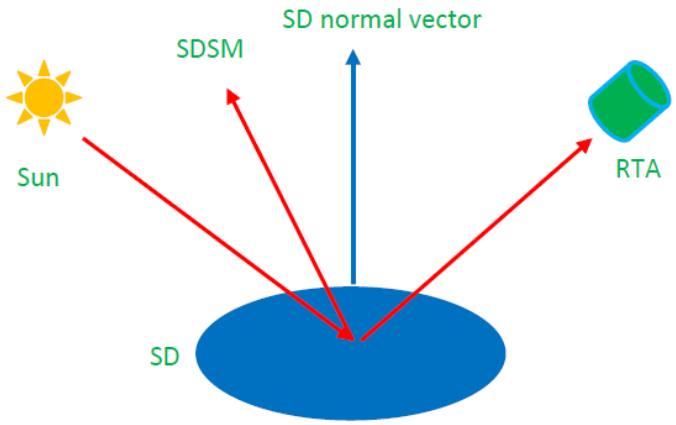

Figure 16. Schematic diagram for SD observation by the SDSM and RTA. The angle between the two views is larger than 100 degrees.

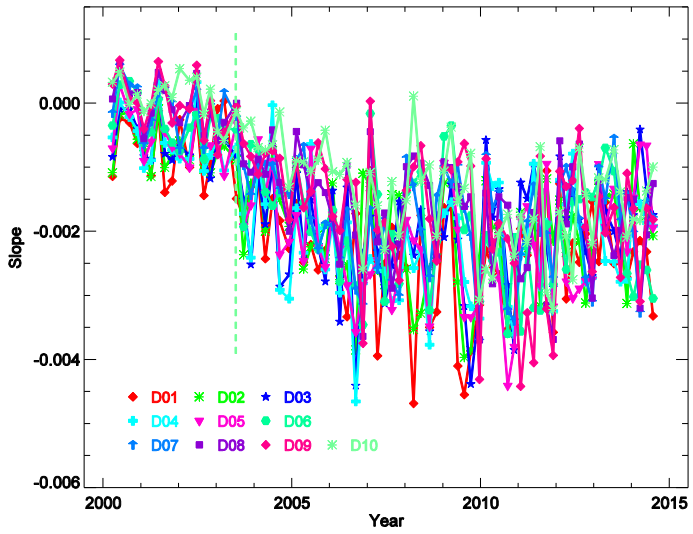

Figure 17. Slopes of the normalized fitted linear functions for Terra band 8 mirror side 1 with SD screen closed.

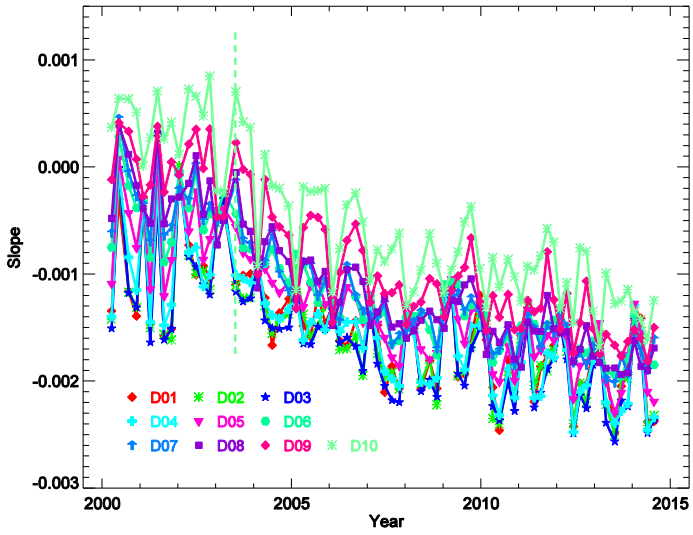

Figure 18. Slopes of the normalized fitted linear functions for Terra band 12 mirror side 1 with SD screen closed.

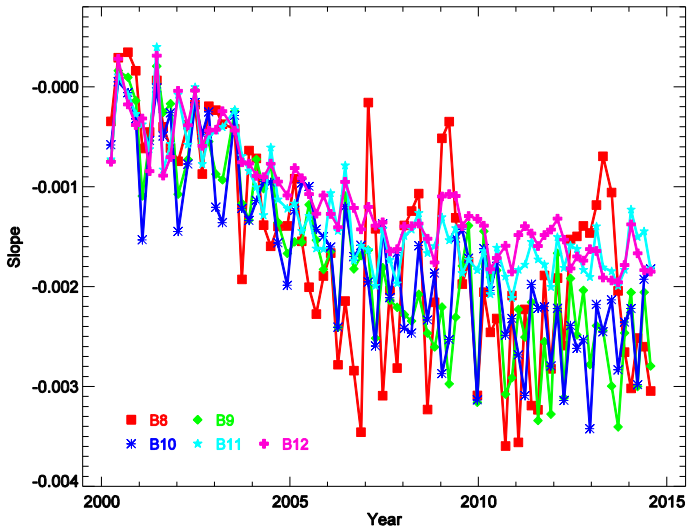

Figure 19. Slopes of the normalized fitted linear functions for Terra bands 8-12 detector 6 mirror side 1 with SD port screen closed.

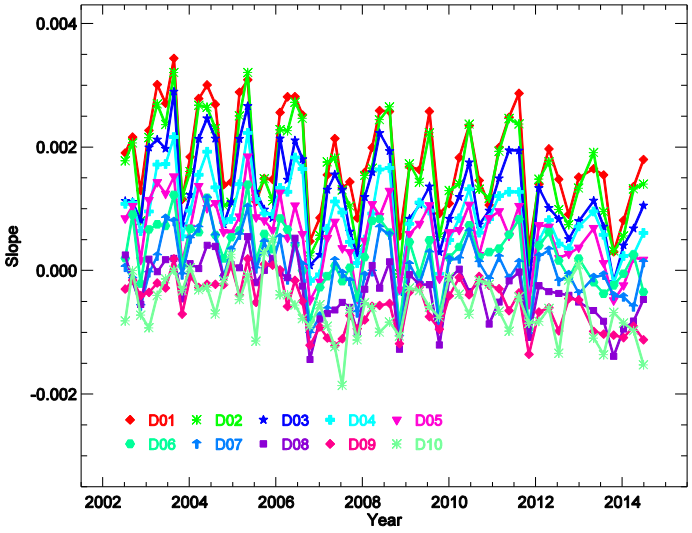

Figure 20. Slopes of the normalized fitted linear functions for Aqua band 8 mirror side 1 with SD screen closed.

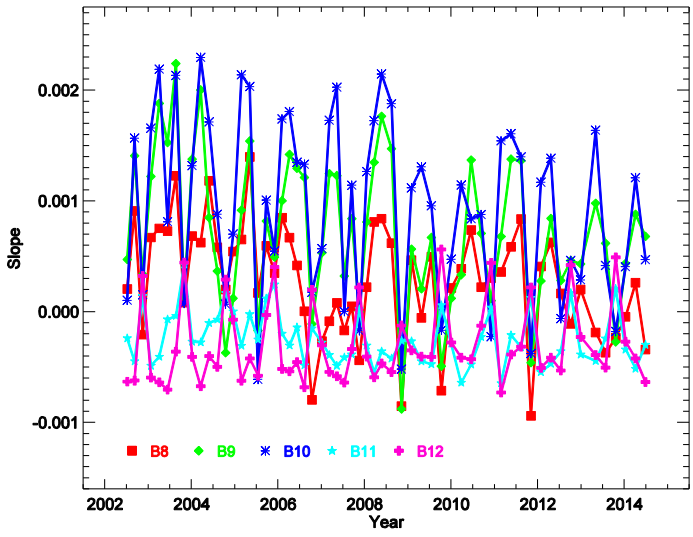

Figure 21. Slopes of the normalized fitted linear functions for Aqua bands 8-12 detector 6 mirror side 1.

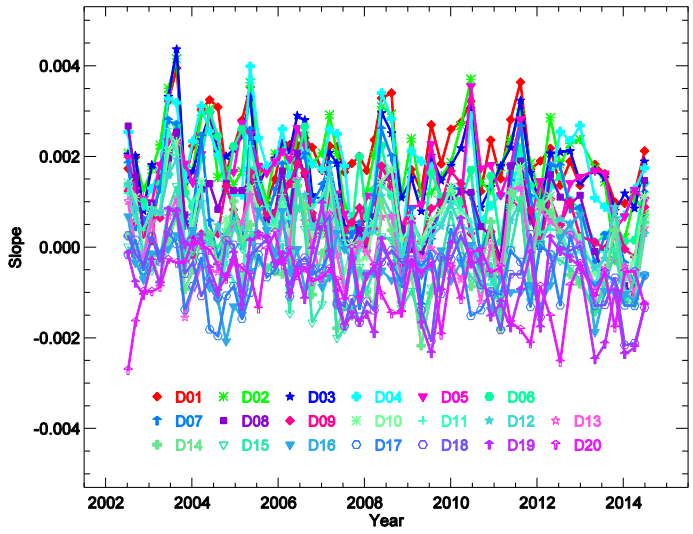

Figure 22. Slopes of the normalized fitted linear functions for Aqua band 3 mirror side 1 with SD screen closed.

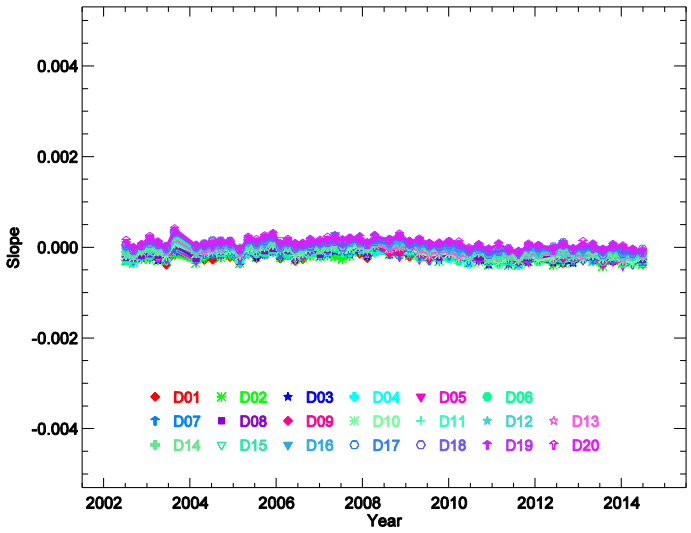

Figure 23. Slopes of the normalized fitted linear functions for Aqua band 3 mirror side 1 with SD screen open.